

Experimental Single-Copy Entanglement Distillation

Sebastian Ecker,^{1,2,*} Philipp Sohr,^{1,2} Lukas Bulla,^{1,2}

Marcus Huber,^{1,3} Martin Bohmann,^{1,2} and Rupert Ursin^{1,2,†}

¹*Institute for Quantum Optics and Quantum Information (IQOQI), Austrian Academy of Sciences, Boltzmannngasse 3, 1090 Vienna, Austria*

²*Vienna Center for Quantum Science and Technology (VCQ), Faculty of Physics, University of Vienna, Boltzmannngasse 5, 1090 Vienna, Austria*

³*Institute for Atomic and Subatomic Physics, Vienna University of Technology, 1020 Vienna, Austria*

The phenomenon of entanglement marks one of the furthest departures from classical physics and is indispensable for quantum information processing. Despite its fundamental importance, the distribution of entanglement over long distances through photons is unfortunately hindered by unavoidable decoherence effects. Entanglement distillation is a means of restoring the quality of such diluted entanglement by concentrating it into a pair of qubits. Conventionally, this would be done by distributing multiple photon pairs and distilling the entanglement into a single pair. Here, we turn around this paradigm by utilising pairs of single photons entangled in multiple degrees of freedom. Specifically, we make use of the polarisation and the energy-time domain of photons, both of which are extensively field-tested. We experimentally chart the domain of distillable states and achieve relative fidelity gains up to 13.8%. Compared to the two-copy scheme, the distillation rate of our single-copy scheme is several orders of magnitude higher, paving the way towards high-capacity and noise-resilient quantum networks.

Entanglement lies at the heart of quantum physics, reflecting the quantum superposition principle between remote subsystems without a classical counterpart. In addition to its fundamental importance, entanglement is an essential resource for most quantum information applications [1], and its distribution between remote parties provides the basis for quantum communication [2], distributed quantum computing [3], and eventually the quantum internet [4]. For entanglement distribution, photons are almost ideal carriers of quantum states. It is possible to create close-to-maximally entangled photon-pairs at high rates in the laboratory [5–8], and recent efforts are venturing out of laboratory environments [9–12], bringing the ultimate goal of a global quantum network within reach. Nonetheless, noise and interaction with the environment are unavoidable, leading to decoherence [13] and the degradation of entanglement.

To counteract such detrimental noise effects, entanglement distillation, also referred to as entanglement purification, was introduced [14, 15]. In entanglement distillation, two copies of a noisy entangled state are employed to distill a single copy with a higher degree of entanglement, a process which can be cascaded until ultimately a pure Bell state is reached. Its implementation is based on two-photon controlled NOT (CNOT) gates [see Fig. S1(a)], and facilitates, for example, quantum repeaters [16–18]. Experimental implementations of entanglement distillation, however, face two challenges: firstly, high optical losses in realistic scenarios lead to low transmission probabilities of a single photon pair [9, 12], let alone the transmission of multiple photon pairs, which substantially limits the distillation rate. Secondly, the required

two-photon CNOT gate cannot be deterministically realised with passive linear optics [19–22]. Therefore, all demonstrations of photonic two-copy entanglement distillation [18, 23–25] are based on a parity check rather than on a genuine CNOT gate.

To overcome these problems, single-copy entanglement distillation was proposed, which harnesses entanglement in different degrees of freedom (DOF) of a single photon pair [26], known as hyperentanglement [27–29]. Instead of operating on two photons, each carrying a qubit, the CNOT gate now acts on two qubits encoded in dif-

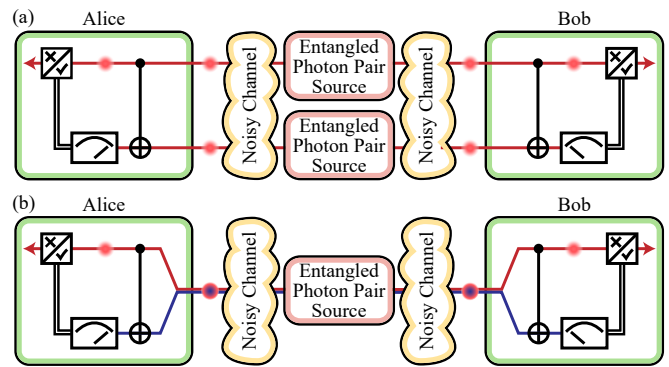


FIG. S1. Schematics of an elementary entanglement distillation step. (a) Two-copy entanglement distillation in which both Alice and Bob apply a CNOT gate between the two single photons they receive. The control photon pair is successfully purified if the measurement outcomes of the target qubits are correlated. (b) Single-copy entanglement distillation employs two entangled subspaces encoded in DOF of a single photon pair. The CNOT gate is now applied between the two DOF and the successful distillation of the control (upper) DOF is heralded by the measurement outcomes of the target (lower) DOF. The classical channel is omitted.

* sebastian.ecker@oeaw.ac.at

† rupert.ursin@oeaw.ac.at

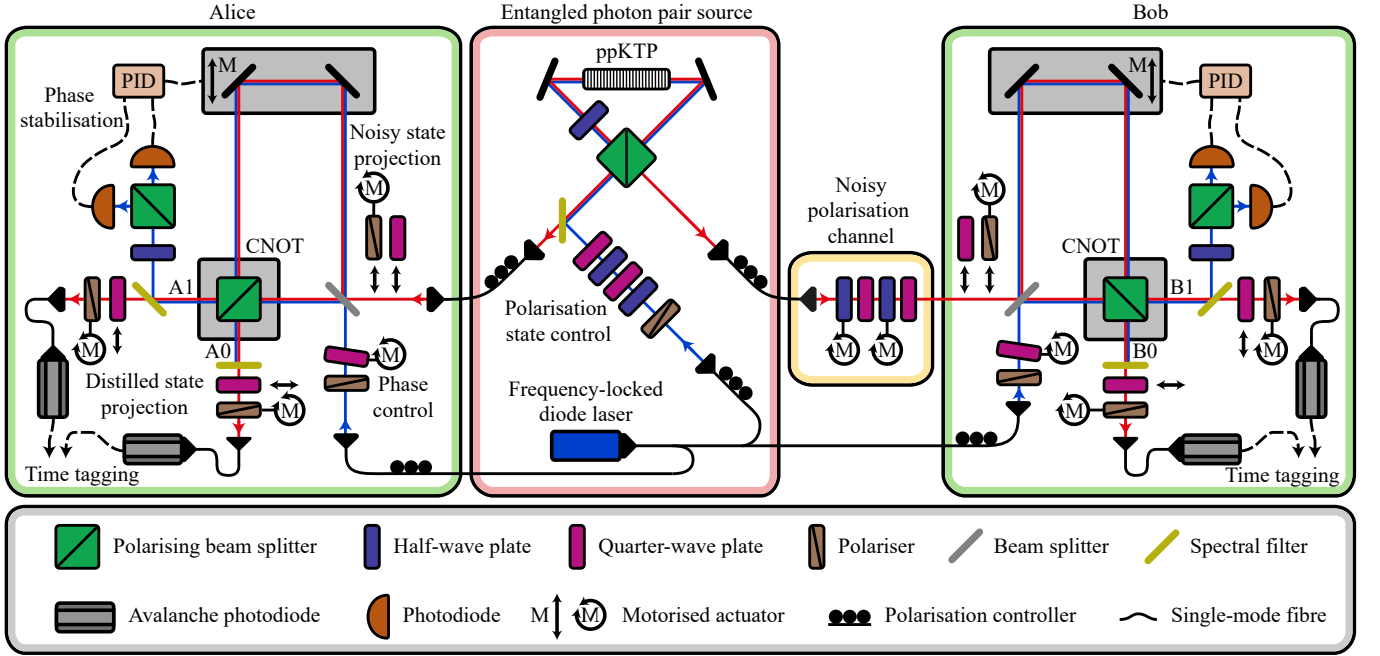


FIG. S2. Experimental setup for single-copy entanglement distillation in polarisation and energy-time. Pairs of entangled photons are created in a periodically-poled potassium titanyl phosphate (ppKTP) crystal placed in a Sagnac interferometer. Polarisation entanglement is produced by bidirectionally pumping the crystal in the interferometer and overlapping the resulting photon-pair modes, while a narrow-line width pump laser gives rise to energy-time entanglement. The entangled photons are single-mode-coupled and guided to Alice and Bob, where the distillation is carried out by interfering the polarisation and the energy-time domain of single photons with a modified Franson interferometer, stabilised by a proportional–integral–derivative (PID) controller. The quantum state is either measured before (Noisy state projection) or after (Distilled state projection) the interferometer and the photons collected in paths A0, A1, B0 and B1 are detected and time-tagged.

ferent DOF of a single photon [see Fig. S1(b)]. Importantly, the CNOT gate between two DOF can be realised deterministically with linear optics [30, 31], which has also been used in a recent purification implementation [32]. Furthermore, hyperentanglement is readily available in spontaneous parametric down-conversion (SPDC) [27, 33] as well as in other photon-pair creating processes [34, 35], and serves as a versatile experimental platform, featuring enhanced communication channel capacity [31, 36, 37]. Notably, the polarisation and the energy-time DOF are particularly robust quantum information carriers and have been distributed over free-space [9, 38, 39] and long-distance fibre [12, 40] links, marking them as ideal candidates for future in-field applications. On the other hand, the originally proposed spatial encoding [26] is less noise resilient outside of a protected laboratory environment [41, 42].

Here, we report the first experimental implementation of a single-copy distillation protocol exploiting hyperentanglement in the field-tested polarisation and energy-time degrees of freedom. We overcome the two principal limitations in standard distillation schemes: the probabilistic nature of multi-photon interactions and the low success rates due to two-pair transmission, both obliterating entangled-photon rates in any realistic scenario. By introducing different noise scenarios at finely tuned noise

levels, we thoroughly test our distillation scheme and successfully recover entanglement and state fidelity. We beat the standard two-copy distillation rate by several orders of magnitude and thus unlock quantum communication in unprecedented noise regimes.

RESULTS

Our experimental platform consists of an entangled photon-pair source, which is connected to the spatially separated communicating parties Alice and Bob via 12m-long single-mode fibres [Fig. S2]. Alice and Bob each have a distillation setup at their disposal and can characterise their part of the entangled quantum state prior to or after the distillation step. We obtain polarisation entanglement in our photon-pair source by superposing a SPDC process in the clockwise and the counterclockwise direction of a Sagnac interferometer [43, 44], creating a superposition of an H-polarised and a V-polarised photon pair. Energy-time entanglement, on the other hand, arises from energy conservation in the SPDC process driven by a temporally coherent pump field, leading to a potentially large superposition of temporal modes $|t_i t_i\rangle$ of the photon pairs [45]. Considering a two-dimensional subspace of the energy-time domain, the resulting hyper-

entangled state we produce is close to

$$|\Phi^+\rangle = \frac{1}{2} [(|H,H\rangle + |V,V\rangle) \otimes (|t_L, t_L\rangle + |t_S, t_S\rangle)], \quad (\text{S.1})$$

where both subspaces are entangled in a Φ^+ Bell state. In order to access the temporal modes at Alice and Bob, we map both photons to the path domain in a Franson interferometer [46] by employing two Mach-Zehnder interferometers with a temporal imbalance of $t_L - t_S$ between the long (L) and the short (S) arm. This mapping is probabilistic due to the randomness of the employed 50:50 beam splitters. Owing to their indistinguishability, only those photon pairs arriving simultaneously at the outputs of the interferometers exhibit quantum interference, requiring postselection on coincidences [47]. The polarising beam splitter at the output ports of the interferometer constitutes the single-photon CNOT gate. Depending on the polarisation state (control qubit) of the photon, the path (target qubit) of the photon is either left unchanged or acted upon with an exclusive OR gate. In analogy with the two-copy distillation protocol [14], the polarisation state is successfully distilled if the measurement outcomes in the computational path basis are correlated. For our experimental setup [Fig. S2], this implies that only photons collected in paths A0 and B0 or A1 and B1 are postselected (see Appendix Sec. A for experimental methods).

In order to fully characterise the performance of the protocol, we separately introduce different error types in the polarisation channel and the energy-time channel. All trace-preserving errors on a qubit can be decomposed into the so-called error basis. Apart from the identity σ_0 , this operator basis consists of the Pauli operators σ_x (bit-flip error), σ_z (phase-flip error) and σ_y (bit-phase-flip error), corresponding to rotations about the three Bloch sphere axes. The error basis is therefore capable of transforming the Φ^+ Bell state into any mixture of Bell states (“Bell-diagonal states”) by means of one-sided transformations. We utilise this fact in the polarisation domain by inserting four waveplates in Bob’s channel (“Noisy polarisation channel”), which introduce arbitrary superpositions in the error basis, and we generate mixed states by averaging over different waveplate settings. The noisy polarisation channel therefore results in a mixture of the Φ^+ state and an erroneous state $\rho_{\text{pol}}^{\text{err}}$. We implement the noisy channel for the energy-time domain by gradually changing the coincidence window, leading to a mixture of the Φ^+ state and an erroneous state $\rho_{\text{e-t}}^{\text{err}} = (|\Psi^+\rangle\langle\Psi^+|_{\text{e-t}} + |\Psi^-\rangle\langle\Psi^-|_{\text{e-t}})/2$ (see Appendix Sec. C and Sec. D for details on the noise control). Owing to the independent manipulation of the polarisation and the energy-time domain, the resulting family of mixed states is still a product state $\rho_{\text{pol}}^{\text{noisy}} \otimes \rho_{\text{e-t}}^{\text{noisy}}$, with

$$\begin{aligned} \rho_{\text{pol}}^{\text{noisy}} &= F_{\text{pol}}^{\text{noisy}} |\Phi^+\rangle\langle\Phi^+|_{\text{pol}} + (1 - F_{\text{pol}}^{\text{noisy}}) \rho_{\text{pol}}^{\text{err}}, \\ \rho_{\text{e-t}}^{\text{noisy}} &= F_{\text{e-t}}^{\text{noisy}} |\Phi^+\rangle\langle\Phi^+|_{\text{e-t}} + (1 - F_{\text{e-t}}^{\text{noisy}}) \rho_{\text{e-t}}^{\text{err}}. \end{aligned}$$

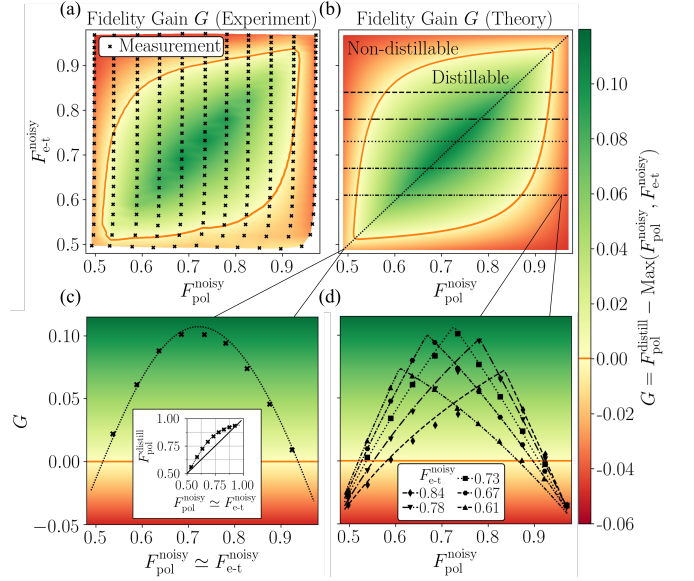


FIG. S3. Fidelity gain after single-copy entanglement distillation in polarisation and energy-time. (a) The gain of the experimental data points are triangulated to form the heat map. Starting from an initial fidelity to the Φ^+ state of $F_{\text{pol}}^{\text{init}} = 97.1\%$ and $F_{\text{e-t}}^{\text{init}} = 96.8\%$ (top right measurement point) we gradually increase the bit-flip (bit and bit-phase-flip) error in polarisation (energy-time) down to a fidelity of $\sim 50\%$. (b) The heat map corresponds to the model, with the initial fidelities and the imperfect CNOT unitary as the only model parameters. (c) A cut through the heat map at $F_{\text{pol}}^{\text{noisy}} \approx F_{\text{e-t}}^{\text{noisy}}$ reveals the characteristic behaviour of two-copy distillation [14]. (d) Cuts through the heat map at constant $F_{\text{e-t}}^{\text{noisy}}$. Both in (c) and (d) lines correspond to the model, while markers correspond to measurement points with a standard deviation smaller than the marker size. The orange line separates the region of distillable ($G > 0$, green) from the region of non-distillable states ($G < 0$, red).

As we are now able to experimentally produce mixed entangled states, we employ them as input to our distillation procedure. The success of the distillation protocol can be evaluated by comparing the noisy and distilled state with each other. For this purpose, we utilise the quantum state fidelity F to the Φ^+ state before and after the distillation. The fidelity is an easily measurable quantity and a good estimator of entanglement [48]. At first, we measure the fidelity $F_{\text{pol}}^{\text{noisy}} = \langle\Phi^+|\rho_{\text{pol}}^{\text{noisy}}|\Phi^+\rangle_{\text{pol}}$ of the noisy polarisation state $\rho_{\text{pol}}^{\text{noisy}}$ to the Φ^+ state and similarly the fidelity $F_{\text{e-t}}^{\text{noisy}}$ of the noisy energy-time state $\rho_{\text{e-t}}^{\text{noisy}}$. After the distillation step

$$\rho_{\text{pol}}^{\text{noisy}} \otimes \rho_{\text{e-t}}^{\text{noisy}} \xrightarrow{\text{distillation}} \rho_{\text{pol}}^{\text{distill}},$$

the fidelity $F_{\text{pol}}^{\text{distill}} = \langle\Phi^+|\rho_{\text{pol}}^{\text{distill}}|\Phi^+\rangle_{\text{pol}}$ of the distilled state $\rho_{\text{pol}}^{\text{distill}}$ to the Φ^+ state determines whether the distillation was successful. Since the single-copy scheme inherently consists of two independent error channels, we make use of the gain $G = F_{\text{pol}}^{\text{distill}} - \text{Max}(F_{\text{pol}}^{\text{noisy}}, F_{\text{e-t}}^{\text{noisy}})$

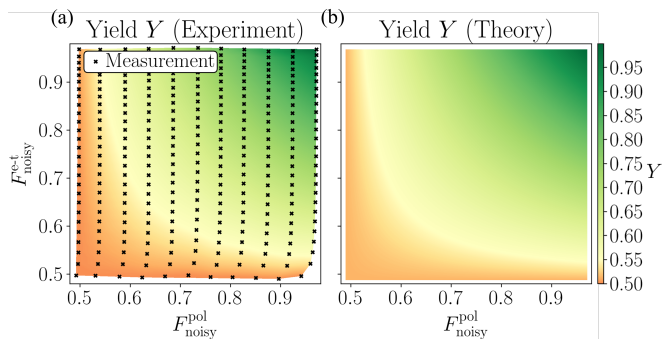


FIG. S4. Yield of single-copy entanglement distillation in polarisation and energy-time. (a) The yield Y corresponds to the measurement in Fig. S3. The heat maps are triangulations of (a) the measurement points and (b) the model data points.

as our figure of merit. Experimentally, the fidelity F to the Φ^+ state is obtained by measuring the interference visibility $V_{ii} = \langle \sigma_i \otimes \sigma_i \rangle$ in three mutually unbiased bases $\{\sigma_x, \sigma_y, \sigma_z\}$, as $F = (1 + V_{xx} - V_{yy} + V_{zz})/4$.

We first introduce a bit-flip error ($\rho_{\text{pol}}^{\text{err}} = |\Psi^+\rangle\langle\Psi^+|_{\text{pol}}$) to the polarisation domain and compare the gain of the experimental data [Fig. S3(a)] with the theory prediction [Fig. S3(b)]. Our experimentally obtained fine-grained error map in Fig. S3 allows us to analyse the performance of the distillation protocol in great detail. Firstly, the region of positive gain ($G > 0$) is approximately symmetrical about the diagonal line defined by $F_{\text{pol}}^{\text{noisy}} \simeq F_{\text{e-t}}^{\text{noisy}}$. All distilled states within this region have a higher fidelity to the maximally entangled Φ_{pol}^+ state than both noisy states before the distillation. The non-distillable states outside of this area ($G < 0$) are highly asymmetric in their error contribution in polarisation and energy-time, while the highest measured gains, up to $G = 0.101$ (13.8% relative gain), can be observed for approximately symmetric error contributions ($F_{\text{pol}}^{\text{noisy}} = 0.734, F_{\text{e-t}}^{\text{noisy}} = 0.732$). A cross-section along the diagonal [Fig. S3(c)] reveals the gain curve known from a bit-flip channel in two-copy entanglement distillation [14] and indicates, in addition to cross-sections at constant energy-time fidelity [Fig. S3(d)], a good agreement between our experimental data and the theory. Another important figure of merit for distillation protocols is the yield. For a single step of the protocol, we define the yield Y as the number of distilled photon pairs divided by the total number of coincident photon pairs. In our experiment, the yield peaks at $Y = 98.6\%$ for states close to the ideal source state in Eq. (S.1), while it does not fall below $Y = 50\%$ for any noisy state (Fig. S4). This is an improvement by a factor of 2 compared to the two-copy distillation protocol, which by default has to sacrifice the target photon pair to herald a successful distillation.

In order to demonstrate the universality of our scheme, we examine the bit-phase-flip error ($\rho_{\text{pol}}^{\text{err}} = |\Psi^-\rangle\langle\Psi^-|_{\text{pol}}$)

as an additional error type. We experimentally observe that this error shows the same gain and yield characteristics as the bit-flip error, and we again obtain a maximal gain of $G = 0.094$ (12.76% relative gain) at approximately symmetric error contributions ($F_{\text{pol}}^{\text{noisy}} = 0.733, F_{\text{e-t}}^{\text{noisy}} = 0.733$). Thus, our results show that single-copy distillation can deal with various noise scenarios.

DISCUSSION

We experimentally demonstrated an entanglement distillation scheme based on interference between the polarisation and the energy-time domain of a single photon pair. Our work constitutes the first experimental realisation of entanglement distillation based on CNOT gates, as initially devised in Refs. [14, 26], between these DOF. By using degrees of freedom which have been widely tested in long-distance experiments, the scheme we introduced can directly be implemented over existing fibre and free-space links. Our thorough analysis of different error types and strengths allowed us to characterise the domain of distillable states and quantify the fidelity gain. These results are of vital importance for future implementations in which, in general, different DOF are faced with different errors during transmission.

Apart from the experimental feasibility of our approach, the major advantage rests upon its high efficiency as compared to two-copy distillation [23]. For typical experimental parameters and link losses of 20 dB in both channels, the single-copy distillation rate outperforms the two-copy scheme by eight orders of magnitude (see Appendix Sec. E for a detailed rate comparison). This illustrates that both the creation and the distribution of multiple photon pairs is costly, while a single hyperentangled photon pair can equivalently be utilised for entanglement distillation using significantly less resources. Additionally, hyperentanglement is naturally produced in SPDC [27] and does not necessarily increase the complexity of photon pair sources, which is essential for the establishment of entanglement distribution infrastructure such as satellite-based entanglement sources [9]. Furthermore, our implementation using the energy-time DOF is more robust in out-of-the-laboratory implementations as compared to realisations using the path DOF [32], which additionally requires modifications of the SPDC source.

As opposed to the two-copy scheme, our experiment neither depends on temporal synchronisation between Alice and Bob at the order of the photon's correlation time [11], nor on the storage in a quantum memory [49]. For quantum cryptography in the polarisation domain, our scheme offers the added advantage of path multiplexing, potentially enhancing the secure key rates significantly [50]. While in its first conception [14, 15], entanglement distillation was thought of as an asymptotic procedure converging on perfectly entangled states, single-copy distillation schemes are of course inherently

limited to a finite number of distillation steps given by the number of accessible DOF (in our case two). Although the observed characteristic of the fidelity gain is evidence of its suitability for recurrence protocols [51], practical considerations make clear that for all known applications in quantum information processing, perfect Bell pairs are not required and usually, crossing a certain noise threshold is sufficient, e.g. for yielding nonzero key rates in quantum key distribution. As our experiment shows, this is where single-copy distillation shows its true power. In low-noise settings, the fidelity gains are moderate, while large gains are obtained in a regime where it really matters—that of high noise. This enables a significant increase in state quality in noise-dominated scenarios, recovering the potential for quantum communication applications in regimes that would otherwise be unattainable.

Photonic hyperentanglement in polarisation and energy-time has already been successfully demonstrated over a free-space link [38], where environmental noise is one of the limiting factors. Our experiment realistically simulates local noise on the polarisation degree of freedom, such as noise from stress-induced polarisation changes in fibres [52]. Additionally, embedding the polarisation state in a higher-dimensional state space of energy-time or spatial modes can lead to the dilution of noise induced by background light or accidental coincidences (isotropic noise) [53]. Thus, combining the noise advantages of higher-dimensional systems with our implemented distillation procedure constitutes a promising path forward.

The presented scheme is, in principle, not limited to photonic implementations, and might be extended to other systems featuring hyperentanglement such as atoms [54] or ions [55]. A natural extension of distillation protocols in two DOF will be the exploitation of

more photonic DOF, enabling multiple distillation steps on a single photon pair. The only prerequisite for including additional entangled DOF is the existence of corresponding CNOT gates [30, 32, 56]. Another viable path is the employment of generalised CNOT gates in high-dimensional entanglement distillation [57].

Distributing entanglement between remote parties in the face of noise is an essential task in quantum information processing. Here, we tackled the problem of inefficient entanglement distillation by exploiting hyperentanglement of a single copy instead of exploiting two copies of a photon pair. Our single-copy entanglement distillation approach enables the distribution of high-fidelity entangled states at practical rates and can thus become a vital building block of a future quantum internet.

ACKNOWLEDGEMENTS

We thank Jan Lang for his support in the photon pair source alignment. We acknowledge funding from the Austrian Science Fund (FWF) through the START project Y879-N27 and from the European Unions Horizon 2020 programme grant agreement No. 857156 (OpenQKD).

AUTHOR CONTRIBUTIONS

S.E., P.S. and R.U. conceived the project; S.E., P.S. and L.B. designed and developed the experiment under the guidance of M.B. and R.U.; S.E., P.S. and L.B. evaluated the experimental data; S.E. wrote the first draft of the manuscript; all authors discussed the results, contributed to writing and reviewed the manuscript; M.B. and R.U. supervised the project.

-
- [1] Mark M Wilde, *Quantum Information Theory* (Cambridge University Press, 2013).
 - [2] Feihu Xu, Xiongfeng Ma, Qiang Zhang, Hoi-Kwong Lo, and Jian-Wei Pan, “Secure quantum key distribution with realistic devices,” *Rev. Mod. Phys.* **92**, 025002 (2020).
 - [3] Daniele Cuomo, Marcello Caleffi, and Angela Sara Cacciapuoti, “Towards a distributed quantum computing ecosystem,” *IET Quantum Communication* **1**, 3–8 (2020).
 - [4] Stephanie Wehner, David Elkouss, and Ronald Hanson, “Quantum internet: A vision for the road ahead,” *Science* **362** (2018).
 - [5] Fabian Steinlechner, Pavel Trojek, Marc Jofre, Henning Weier, Daniel Perez, Thomas Jennewein, Rupert Ursin, John Rarity, Morgan W. Mitchell, Juan P. Torres, Harald Weinfurter, and Valerio Pruneri, “A high-brightness source of polarization-entangled photons optimized for applications in free space,” *Opt. Express* **20**, 9640–9649 (2012).
 - [6] Yuanyuan Chen, Sebastian Ecker, Sören Wengerowsky, Lukas Bulla, Siddarth Koduru Joshi, Fabian Steinlechner, and Rupert Ursin, “Polarization entanglement by time-reversed hong-ou-mandel interference,” *Phys. Rev. Lett.* **121**, 200502 (2018).
 - [7] Sebastian Ecker, Bo Liu, Johannes Handsteiner, Matthias Fink, Dominik Rauch, Fabian Steinlechner, Thomas Scheidl, Anton Zeilinger, and Rupert Ursin, “Strategies for achieving high key rates in satellite-based qkd,” *npj Quantum Information* **7**, 1–7 (2021).
 - [8] Michael Kues, Christian Reimer, Piotr Roztock, Luis Romero Cortés, Stefania Sciara, Benjamin Wetz, Yanbing Zhang, Alfonso Cino, Sai T Chu, Brent E Little, *et al.*, “On-chip generation of high-dimensional entangled quantum states and their coherent control,” *Nature* **546**, 622–626 (2017).
 - [9] Juan Yin, Yuan Cao, Yu-Huai Li, Sheng-Kai Liao, Liang Zhang, Ji-Gang Ren, Wen-Qi Cai, Wei-Yue Liu, Bo Li,

- Hui Dai, Guang-Bing Li, Qi-Ming Lu, Yun-Hong Gong, Yu Xu, Shuang-Lin Li, Feng-Zhi Li, Ya-Yun Yin, Zi-Qing Jiang, Ming Li, Jian-Jun Jia, Ge Ren, Dong He, Yi-Lin Zhou, Xiao-Xiang Zhang, Na Wang, Xiang Chang, Zhen-Cai Zhu, Nai-Le Liu, Yu-Ao Chen, Chao-Yang Lu, Rong Shu, Cheng-Zhi Peng, Jian-Yu Wang, and Jian-Wei Pan, “Satellite-based entanglement distribution over 1200 kilometers,” *Science* **356**, 1140–1144 (2017).
- [10] Siddharth Koduru Joshi, Djeylan Aktas, Sören Wengerowsky, Martin Lončarić, Sebastian Philipp Neumann, Bo Liu, Thomas Scheidl, Guillermo Currás Lorenzo, Željko Samec, Laurent Kling, Alex Qiu, Mohsen Razavi, Mario Stipčević, John G. Rarity, and Rupert Ursin, “A trusted node-free eight-user metropolitan quantum communication network,” *Science Advances* **6** (2020), 10.1126/sciadv.aba0959.
- [11] Raju Valivarthi, Qiang Zhou, Gabriel H Aguilar, Varun B Verma, Francesco Marsili, Matthew D Shaw, Sae Woo Nam, Daniel Oblak, Wolfgang Tittel, *et al.*, “Quantum teleportation across a metropolitan fibre network,” *Nature Photonics* **10**, 676–680 (2016).
- [12] Sören Wengerowsky, Siddharth Koduru Joshi, Fabian Steinlechner, Julien R. Zichi, Sergiy M. Dobrovolskiy, René van der Molen, Johannes W. N. Los, Val Zwiller, Marijn A. M. Versteegh, Alberto Mura, Davide Calonico, Massimo Inguscio, Hannes Hübel, Liu Bo, Thomas Scheidl, Anton Zeilinger, André Xuereb, and Rupert Ursin, “Entanglement distribution over a 96-km-long submarine optical fiber,” *Proceedings of the National Academy of Sciences* **116**, 6684–6688 (2019).
- [13] Maximilian Schlosshauer, “Quantum decoherence,” *Physics Reports* **831**, 1 – 57 (2019).
- [14] Charles H. Bennett, Gilles Brassard, Sandu Popescu, Benjamin Schumacher, John A. Smolin, and William K. Wootters, “Purification of noisy entanglement and faithful teleportation via noisy channels,” *Phys. Rev. Lett.* **76**, 722–725 (1996).
- [15] David Deutsch, Artur Ekert, Richard Jozsa, Chiara Macchiavello, Sandu Popescu, and Anna Sanpera, “Quantum privacy amplification and the security of quantum cryptography over noisy channels,” *Phys. Rev. Lett.* **77**, 2818–2821 (1996).
- [16] H.-J. Briegel, W. Dür, J. I. Cirac, and P. Zoller, “Quantum repeaters: The role of imperfect local operations in quantum communication,” *Phys. Rev. Lett.* **81**, 5932–5935 (1998).
- [17] W. Dür, H.-J. Briegel, J. I. Cirac, and P. Zoller, “Quantum repeaters based on entanglement purification,” *Phys. Rev. A* **59**, 169–181 (1999).
- [18] Luo-Kan Chen, Hai-Lin Yong, Ping Xu, Xing-Can Yao, Tong Xiang, Zheng-Da Li, Chang Liu, He Lu, Nai-Le Liu, Li Li, *et al.*, “Experimental nested purification for a linear optical quantum repeater,” *Nature Photonics* **11**, 695–699 (2017).
- [19] Jeremy L O’Brien, Geoffrey J Pryde, Andrew G White, Timothy C Ralph, and David Branning, “Demonstration of an all-optical quantum controlled-not gate,” *Nature* **426**, 264–267 (2003).
- [20] T. B. Pittman, M. J. Fitch, B. C Jacobs, and J. D. Franson, “Experimental controlled-not logic gate for single photons in the coincidence basis,” *Phys. Rev. A* **68**, 032316 (2003).
- [21] Sara Gasparoni, Jian-Wei Pan, Philip Walther, Terry Rudolph, and Anton Zeilinger, “Realization of a photonic controlled-not gate sufficient for quantum computation,” *Phys. Rev. Lett.* **93**, 020504 (2004).
- [22] Zhi Zhao, An-Ning Zhang, Yu-Ao Chen, Han Zhang, Jiang-Feng Du, Tao Yang, and Jian-Wei Pan, “Experimental demonstration of a nondestructive controlled-not quantum gate for two independent photon qubits,” *Phys. Rev. Lett.* **94**, 030501 (2005).
- [23] Jian-Wei Pan, Sara Gasparoni, Rupert Ursin, Gregor Weihs, and Anton Zeilinger, “Experimental entanglement purification of arbitrary unknown states,” *Nature* **423**, 417–422 (2003).
- [24] Takashi Yamamoto, Masato Koashi, Şahin Kaya Özdemir, and Nobuyuki Imoto, “Experimental extraction of an entangled photon pair from two identically decohered pairs,” *Nature* **421**, 343–346 (2003).
- [25] P. Walther, K. J. Resch, Č. Brukner, A. M. Steinberg, J.-W. Pan, and A. Zeilinger, “Quantum nonlocality obtained from local states by entanglement purification,” *Phys. Rev. Lett.* **94**, 040504 (2005).
- [26] Christoph Simon and Jian-Wei Pan, “Polarization entanglement purification using spatial entanglement,” *Phys. Rev. Lett.* **89**, 257901 (2002).
- [27] Julio T. Barreiro, Nathan K. Langford, Nicholas A. Peters, and Paul G. Kwiat, “Generation of hyperentangled photon pairs,” *Phys. Rev. Lett.* **95**, 260501 (2005).
- [28] M. Barbieri, C. Cinelli, P. Mataloni, and F. De Martini, “Polarization-momentum hyperentangled states: Realization and characterization,” *Phys. Rev. A* **72**, 052110 (2005).
- [29] Xi-Han Li and Shohini Ghose, “Complete hyperentangled bell state analysis for polarization and time-bin hyperentanglement,” *Opt. Express* **24**, 18388–18398 (2016).
- [30] Marco Fiorentino and Franco N. C. Wong, “Deterministic controlled-not gate for single-photon two-qubit quantum logic,” *Phys. Rev. Lett.* **93**, 070502 (2004).
- [31] Julio T Barreiro, Tzu-Chieh Wei, and Paul G Kwiat, “Beating the channel capacity limit for linear photonic superdense coding,” *Nature physics* **4**, 282–286 (2008).
- [32] Xiao-Min Hu, Cen-Xiao Huang, Yu-Bo Sheng, Lan Zhou, Bi-Heng Liu, Yu Guo, Chao Zhang, Wen-Bo Xing, Yun-Feng Huang, Chuan-Feng Li, and Guang-Can Guo, “Long-distance entanglement purification for quantum communication,” *Phys. Rev. Lett.* **126**, 010503 (2021).
- [33] Paul G. Kwiat, “Hyper-entangled states,” *Journal of Modern Optics* **44**, 2173–2184 (1997).
- [34] Maximilian Prilmüller, Tobias Huber, Markus Müller, Peter Michler, Gregor Weihs, and Ana Predojević, “Hyperentanglement of photons emitted by a quantum dot,” *Phys. Rev. Lett.* **121**, 110503 (2018).
- [35] Christian Reimer, Stefania Sciara, Piotr Roztocki, Mehedi Islam, Luis Romero Cortés, Yanbing Zhang, Bennet Fischer, Sébastien Loranger, Raman Kashyap, Alfonso Cino, *et al.*, “High-dimensional one-way quantum processing implemented on d-level cluster states,” *Nature Physics* **15**, 148–153 (2019).
- [36] Trent M Graham, Herbert J Bernstein, Tzu-Chieh Wei, Marius Junge, and Paul G Kwiat, “Superdense teleportation using hyperentangled photons,” *Nature communications* **6**, 1–9 (2015).
- [37] Brian P. Williams, Ronald J. Sadler, and Travis S. Humble, “Superdense coding over optical fiber links with complete bell-state measurements,” *Phys. Rev. Lett.* **118**, 050501 (2017).

- [38] Fabian Steinlechner, Sebastian Ecker, Matthias Fink, Bo Liu, Jessica Bavaresco, Marcus Huber, Thomas Scheidl, and Rupert Ursin, “Distribution of high-dimensional entanglement via an intra-city free-space link,” *Nature communications* **8**, 15971 (2017).
- [39] Jeongwan Jin, Jean-Philippe Bourgoin, Ramy Tannous, Sascha Agne, Christopher J. Pugh, Katanya B. Kuntz, Brendon L. Higgins, and Thomas Jennewein, “Genuine time-bin-encoded quantum key distribution over a turbulent depolarizing free-space channel,” *Opt. Express* **27**, 37214–37223 (2019).
- [40] I. Marcikic, H. de Riedmatten, W. Tittel, H. Zbinden, M. Legré, and N. Gisin, “Distribution of time-bin entangled qubits over 50 km of optical fiber,” *Phys. Rev. Lett.* **93**, 180502 (2004).
- [41] Mario Krenn, Johannes Handsteiner, Matthias Fink, Robert Fickler, and Anton Zeilinger, “Twisted photon entanglement through turbulent air across vienna,” *Proceedings of the National Academy of Sciences* **112**, 14197–14201 (2015).
- [42] B. Da Lio, D. Bacco, D. Cozzolino, N. Biagi, T. N. Arge, E. Larsen, K. Rottwitt, Y. Ding, A. Zavatta, and L. K. Oxenløwe, “Stable transmission of high-dimensional quantum states over a 2-km multicore fiber,” *IEEE Journal of Selected Topics in Quantum Electronics* **26**, 1–8 (2020).
- [43] Taehyun Kim, Marco Fiorentino, and Franco N. C. Wong, “Phase-stable source of polarization-entangled photons using a polarization sagnac interferometer,” *Phys. Rev. A* **73**, 012316 (2006).
- [44] Alessandro Fedrizzi, Thomas Herbst, Andreas Poppe, Thomas Jennewein, and Anton Zeilinger, “A wavelength-tunable fiber-coupled source of narrow-band entangled photons,” *Opt. Express* **15**, 15377–15386 (2007).
- [45] Anthony Martin, Thiago Guerreiro, Alexey Tiranov, Sébastien Designolle, Florian Fröwis, Nicolas Brunner, Marcus Huber, and Nicolas Gisin, “Quantifying photonic high-dimensional entanglement,” *Phys. Rev. Lett.* **118**, 110501 (2017).
- [46] J. D. Franson, “Bell inequality for position and time,” *Phys. Rev. Lett.* **62**, 2205–2208 (1989).
- [47] P. G. Kwiat, A. M. Steinberg, and R. Y. Chiao, “High-visibility interference in a bell-inequality experiment for energy and time,” *Phys. Rev. A* **47**, R2472–R2475 (1993).
- [48] Nicolai Friis, Giuseppe Vitagliano, Mehul Malik, and Marcus Huber, “Entanglement certification from theory to experiment,” *Nature Reviews Physics* **1**, 72–87 (2019).
- [49] Alessandro Seri, Andreas Lenhard, Daniel Rieländer, Mustafa Gündoğan, Patrick M. Ledingham, Margherita Mazzera, and Hugues de Riedmatten, “Quantum correlations between single telecom photons and a multimode on-demand solid-state quantum memory,” *Phys. Rev. X* **7**, 021028 (2017).
- [50] Johannes Pseiner, Lukas Achatz, Lukas Bulla, Martin Bohmann, and Rupert Ursin, “Experimental wavelength-multiplexed entanglement-based quantum cryptography,” *arXiv preprint arXiv:2009.03691* (2020).
- [51] Charles H. Bennett, David P. DiVincenzo, John A. Smolin, and William K. Wootters, “Mixed-state entanglement and quantum error correction,” *Phys. Rev. A* **54**, 3824–3851 (1996).
- [52] Alexander Treiber, Andreas Poppe, Michael Hentschel, Daniele Ferrini, Thomas Lorünser, Edwin Querasser, Thomas Matyus, Hannes Hübel, and Anton Zeilinger, “A fully automated entanglement-based quantum cryptography system for telecom fiber networks,” *New Journal of Physics* **11**, 045013 (2009).
- [53] Sebastian Ecker, Frédéric Bouchard, Lukas Bulla, Florian Brandt, Oskar Kohout, Fabian Steinlechner, Robert Fickler, Mehul Malik, Yelena Guryanova, Rupert Ursin, and Marcus Huber, “Overcoming noise in entanglement distribution,” *Phys. Rev. X* **9**, 041042 (2019).
- [54] Mehwish Nawaz, Rameez ul Islam, Tasawar Abbas, and Manzoor Ikram, “Engineering quantum hyperentangled states in atomic systems,” *Journal of Physics B: Atomic, Molecular and Optical Physics* **50**, 215502 (2017).
- [55] Bao-Lin Hu and You-Bang Zhan, “Generation of hyperentangled states between remote noninteracting atomic ions,” *Phys. Rev. A* **82**, 054301 (2010).
- [56] Florian Brandt, Markus Hiekkamäki, Frédéric Bouchard, Marcus Huber, and Robert Fickler, “High-dimensional quantum gates using full-field spatial modes of photons,” *Optica* **7**, 98–107 (2020).
- [57] J. Miguel-Ramiro and W. Dür, “Efficient entanglement purification protocols for d -level systems,” *Phys. Rev. A* **98**, 042309 (2018).

APPENDIX

In this Appendix we describe our experimental methods, provide a detailed analysis of the modified Franson interferometer and illustrate the introduction of noise to the energy-time degree of freedom. The Appendix is organised as follows. In Sec. A, we describe our experimental setup and detail the employed methods. In Sec. B, we discuss the working principle of the distillation setup and show how the two polarising beamsplitters act as a bilateral CNOT gate between the polarisation and the energy-time degree of freedom. The influence of the coincidence window is discussed in Sec. C. In Sec. D, we show how the error contribution in the energy-time degree of freedom can be controlled and how it affects the distillation. In Sec. E, we compare the distillation rate of the single-copy protocol with the two-copy protocol.

Appendix A: Experimental Methods

A1. Entangled photon pair source

We produce photon pairs in spontaneous parametric down-conversion (SPDC) with type-II phase-matching by tightly focusing a continuous-wave pump beam into a 30-mm-long periodically-poled potassium titanyl phosphate (ppKTP) crystal. The ppKTP crystal is temperature-tuned for degenerate phase-matching, yielding a centre wavelength of 809.1 nm for the down-converted photons. The pump laser (Toptica DL pro) is externally frequency-stabilised by locking it to a hyperfine transition of ^{39}K , utilising Doppler-free spectroscopy, resulting in a wavelength stability of ~ 0.6 fm/min at a wavelength of 404.53 nm. Polarisation entanglement is obtained by bidirectionally pumping the ppKTP crystal within a polarisation Sagnac interferometer. The entangled polarisation state can be controlled by a series of waveplates in the pump beam. The photons are detected with avalanche photodiodes (Excelitas Technologies SPCM-800-11-FC) and each detection event is timestamped with a time-tagger (Swabian Instruments - Time Tagger Ultra). A high degree of polarisation entanglement is accomplished by a good spatiotemporal overlap of the two SPDC processes, with typical interference visibilities of $V_{\text{H/V}} = 99.9\%$ and $V_{\text{D/A}} = 97.8\%$ in the rectilinear and diagonal polarisation basis, respectively. After single-mode coupling we observe a photon-pair rate of 68 kcps per mW of pump power at a symmetric heralding efficiency of $\sim 24\%$.

A2. Franson interferometer

The two imbalanced Mach-Zehnder interferometers are stabilised by the frequency-locked pump laser. Active phase stabilisation is achieved by a proportional–integral–derivative (PID) control loop of the difference signal from two photodiodes and a piezoactuator displacing both long arm mirrors. The stabilisation laser is injected into the unused port of the beam splitter and retrieved by a dichroic mirror after the interferometer, where the polarisation contrast is measured by fast photodiodes in a polarisation basis conjugate to the interferometer-defined polarisation basis. Phase-control is accomplished by tilting a multi-order waveplate in the pump beam, forcing the control loop to follow its setpoint. The time delay between the long and the short arm of the Mach-Zehnder interferometer is 2.6 ns, which is larger than the FWHM timing-jitter of the detection system (~ 800 ps) and smaller than the coherence time of the pump laser (~ 600 ns).

A3. Noisy channel

In polarisation, we introduce errors by a sequence of four waveplates (“Noisy polarisation channel”). The relative rotation angles of the waveplates both determine the error type and the error contribution. We generate mixed entangled polarisation states by alternately setting the corresponding waveplate of the noisy polarisation channel to $+\theta$ and $-\theta$, with the neutral angle at $\theta = 0$, leading to a reduction of coherences in the resulting state. The controlled introduction of errors in the energy-time domain is more involved due to the lack of easy-to-implement unitaries. We make use of the non-interfering states $|t_L, t_S\rangle \langle t_L, t_S|$ and $|t_S, t_L\rangle \langle t_S, t_L|$, which are usually discarded in coincidence postselection. These admixtures correspond to a combined bit- and bit-phase-flip error $(|\Psi^+\rangle \langle \Psi^+|_{\text{e-t}} + |\Psi^-\rangle \langle \Psi^-|_{\text{e-t}})/2$. The error proportion can be tuned by gradually changing the coincidence window duration.

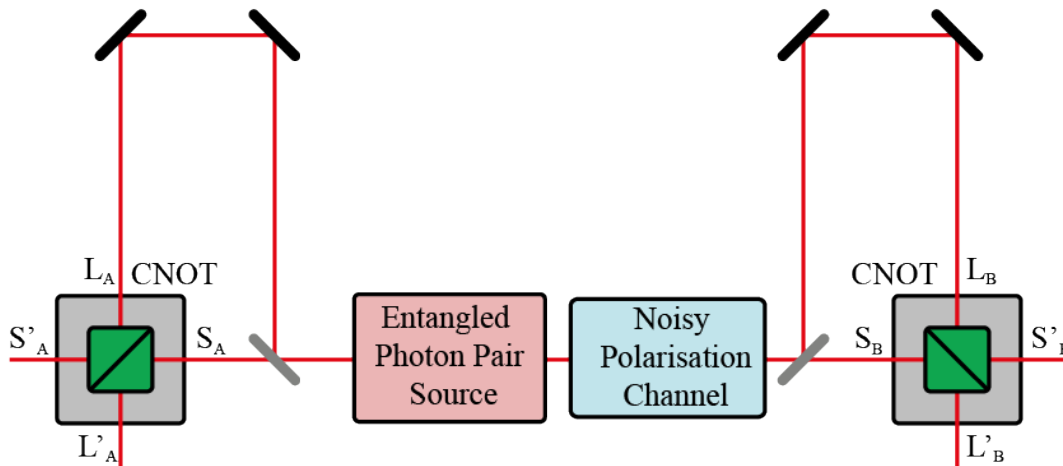


FIG. S5. Simplified setup scheme. The basic structure of our distillation setup is a modified Franson interferometer [46]. While the input BS remain, the output BS are replaced by PBS as compared to the original scheme. The short paths in the unbalanced Mach-Zehnder interferometers are labelled with S_A and S_B at Alice’s and Bob’s side respectively. The long paths are labelled with L_A and L_B . The modes transmitted by the PBS are marked with a dash. Locally, each PBS acts as CNOT gate with the polarisation DOF as control and the e-t (path) DOF as target. The polarisation mode H can be associated with the logical state 0 and the polarisation mode V can be associated with the logical state 1, i.e., the path mode is flipped if the photon incident on the PBS is vertically polarised and it remains unchanged if the photon is horizontally polarised. The joint action of both polarising beam splitters is a bilateral CNOT. (BS: beam splitter, CNOT: controlled NOT, DOF: degree of freedom, PBS: polarising beam splitter)

A4. Fidelity measurements

Different fidelity measurements require minor changes to the detection part of the setup. For $F_{\text{pol}}^{\text{noisy}}$ we insert the polariser (“Noisy state projection”) in front of the interferometer and block the long arm to prevent interference. The polarisers after the interferometer (“Distilled state projection”) are set to maximal transmission. The two linear polarisation bases $\{H,V\}$ and $\{D,A\}$ (σ_z and σ_x) can now be accessed by rotating the polariser. After inserting a quarter wave plate in front of the polariser, the circular polarisation basis $\{R,L\}$ (σ_y) can be accessed. For the measurement of $F_{\text{e-t}}^{\text{noisy}}$, the long arm is unblocked. We measure in the computational basis $\{t_L, t_S\}$ (σ_z) by setting both the noisy and distilled state projection polarisers at H-polarisation. Accessing the superposition bases $\{t_L \pm t_S\}$ and $\{t_L \pm it_S\}$ (σ_x and σ_y) is accomplished by setting both the noisy and distilled state projection polarisers at D-polarisation. The phase corresponding to each of the two bases is set via the phase control waveplate. The distilled fidelity $F_{\text{pol}}^{\text{distill}}$ is measured by removing the noisy state projection polarisers entirely. In total, each measurement point in main text Fig. 3 requires 54 different measurement settings, with an integration time of 10 s per setting, amounting to 594 settings overall. The coincidence rates at different coincidence windows are computed in post-processing. For large coincidence windows, the polarisation fidelity $F_{\text{pol}}^{\text{noisy}}$ seems to get worse, especially for high fidelities (see main text Fig. 3a). This is due to a back-reflection during single-mode coupling in the photon pair source. The back-reflected photons make one additional round trip in the Sagnac interferometer, which agrees with the relative time delay we observe.

Appendix B: Working principle of the setup and bilateral CNOT gate

The energy-time (e-t) degree of freedom (DOF) distributed from the entangled-photon-pair source is analysed in a two-dimensional subspace by a Franson-type interferometer sketched in Figure S5. Each balanced beamsplitter (BS) splits one input mode into two path modes, which serve as input modes for the polarising BS (PBS), closing the imbalanced Mach-Zehnder interferometer. The two paths are not only characterised by their length L_A and L_B , but also by the propagation time of the photons t_{L_A} and t_{L_B} , such that e.g., $L_A = c t_{L_A}$, with the speed of light c . Hence, there is a direct relation between the path and the e-t DOF. In the following, we will use the path labels, while still referring to the e-t DOF. When discussing the action of the PBS, we will keep track of the time separately.

The path length difference in each Mach-Zehnder interferometer, that is $\Delta L_A \equiv L_A - S_A$ at Alice’s (A) side and

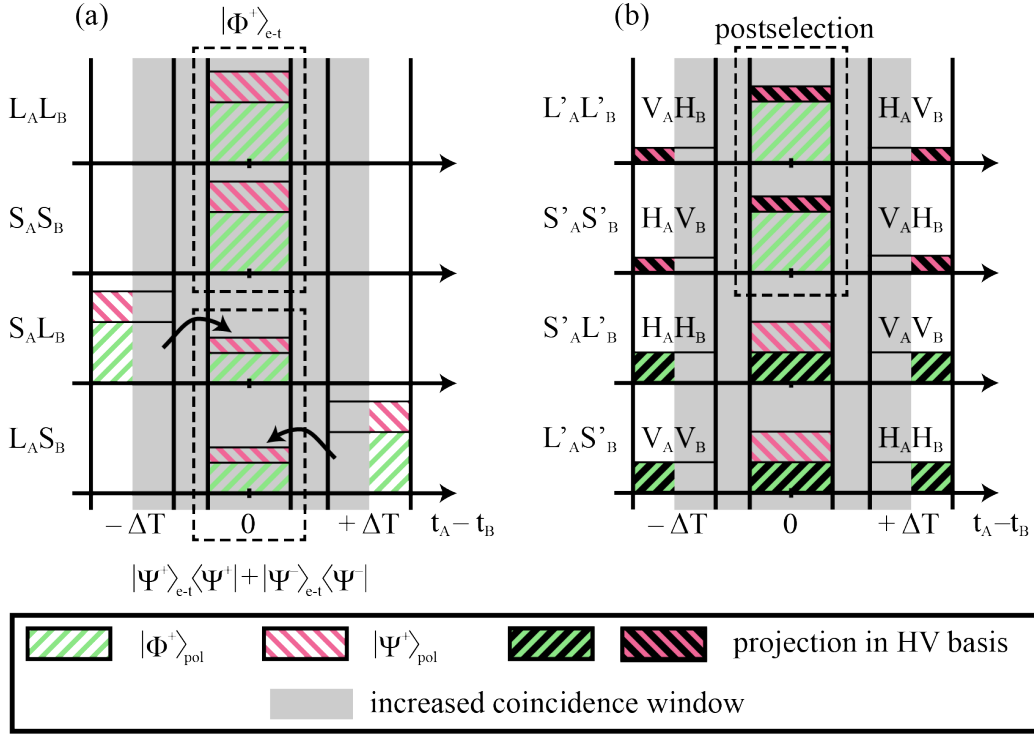


FIG. S6. Delay histogram visualising the effect of an increased coincidence window on the two-photon state in both the polarisation and the energy time DOF before (a) and after (b) the bCNOT. The state in the e-t DOF is depicted by 12 slots spanned by three orthogonal states with relative time delays $-\Delta T$, 0 and ΔT and four orthogonal path states. The polarisation state is depicted by hatched regions, where the proportion of the regions represent the proportion of the contributions to the mixed state. We consider the target state Φ_{pol}^+ with an admixed bit flip contribution Ψ_{pol}^+ . The initial amount of bit flip error in polarisation as well as the width of the coincidence window are chosen arbitrarily. After the distillation (b), which includes the action of the bCNOT as well as the postselection on the $\Phi_{\text{e-t}}^\pm$ states in the e-t DOF, the unwanted contributions are clearly reduced compared to the input polarisation state before the bCNOT (a). A detailed description of the state evolution is given in the text. (bCNOT: bilateral controlled NOT, DOF: degree of freedom)

$\Delta L_B \equiv L_B - S_B$ at Bob's side, introduces a time delay. These time delays should be well between the single-photon coherence time τ_{sp} and the coherence time of the pump laser τ_{pump}

$$\tau_{\text{sp}} \ll \frac{\Delta L_i}{c} \ll \tau_{\text{pump}}, \quad (\text{S.1})$$

with $i \in \{A, B\}$. The lower limit on the imbalance ensures that no single photon interference is observed locally at A or B, while the upper limit on the imbalance ensures the coherence of the possible two-photon modes $S_A S_B$, $S_A L_B$, $L_A S_B$ and $L_A L_B$. If further the interferometer imbalances at A and B are the same ($\Delta L_A = \Delta L_B$), the modes $S_A S_B$ and $L_A L_B$ are indistinguishable by their relative time delay $t_A - t_B \equiv 0$. The remaining modes $S_A L_B$ and $L_A S_B$, on the contrary, are clearly distinguishable by their time delays $t_A - t_B \equiv -\Delta T$ and ΔT respectively. In a delay histogram as shown in Fig. S6a, they form the side-peaks centred around the central-peak at time delay 0.

Appendix C: Influence of the coincidence window

By choosing the time window for coincidence counting small enough, the side peaks can be excluded in post-processing, such that the Bell state $|\Phi^+\rangle_{\text{e-t}} = (|S_A S_B\rangle + |L_A L_B\rangle) / \sqrt{2}$ can be prepared if the phases in the long paths are adjusted. The Φ^+ state is of particular interest, as the contribution of Φ^+ states in both DOF remains unchanged under the joint action of the PBS. As each PBS acts as a CNOT gate between the polarisation DOF and the e-t DOF, we will call the joint action of both PBS a bilateral CNOT (bCNOT).

In Figure S6a, the effect of an increased coincidence window on the state before the distillation step is illustrated.

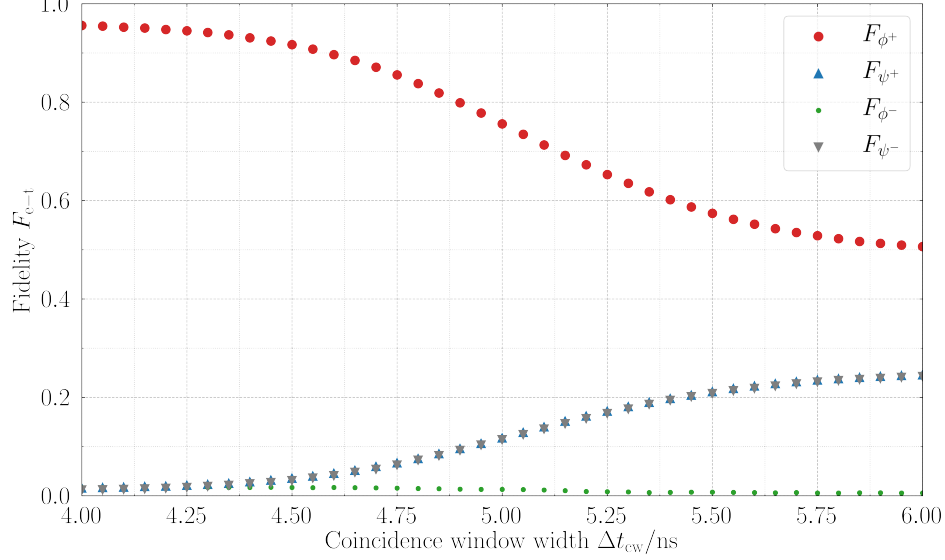


FIG. S7. Experimental data of the Bell state fidelities in the e-t DOF before the bCNOT as a function of the coincidence window width. With an increasing coincidence window, the fidelities to the Ψ^\pm states rise equally up to 0.25 once the side-peaks are fully included in the coincidence window. At the same time, the fidelity to the target state of the distillation process Φ^+ declines to 0.5. The fidelity to the Ψ^- state is non-zero due to residual phase errors. The error bars are too small to be shown. (bCNOT: bilateral controlled NOT, DOF: degree of freedom, e-t: energy-time)

If the coincidence window partially includes the side-peaks, both the central-peak, as well as parts of the side-peak are identified as coincidence by the logic. However, since contributions from the side-peaks are in principle physically distinguishable by their relative time delay, they form a non-interfering background. In case of an equal contribution of the side-peaks, the non-interfering background is proportional to a balanced mixture of the Ψ_{e-t}^\pm states

$$|S_A L_B\rangle\langle S_A L_B| + |L_A S_B\rangle\langle L_A S_B| = |\Psi^+\rangle_{e-t}\langle\Psi^+| + |\Psi^-\rangle_{e-t}\langle\Psi^-|. \quad (\text{S.1})$$

In Figure S7 we gradually increased the coincidence window of experimental data, and indeed found an increasing admixture of the states in Eq. (S.1). While the illustration by the histogram (see Fig. (S6)) might give the impression that there is a linear relation between the coincidence window width and the Bell state fidelity in the e-t DOF, the experimental data show that this is not the case. Instead, the experimental data reflects the Gaussian shape of the coincidence peaks governed by the timing jitter of the photon detectors.

Appendix D: Energy-time noise in the distillation protocol

So far, the polarisation DOF did not play a role. This changes once we consider the effect of the bCNOT, as it is implemented by two polarising beam splitters. Each PBS acts as CNOT between with the polarisation DOF as control qubit and the path DOF as target qubit, e.g.,

$$|H\rangle_{\text{pol}} \otimes |S_A\rangle_{e-t} \xrightarrow{\text{CNOT}} |H\rangle_{\text{pol}} \otimes |S'_A\rangle_{e-t}, \quad (\text{S.1})$$

$$|H\rangle_{\text{pol}} \otimes |L_A\rangle_{e-t} \xrightarrow{\text{CNOT}} |H\rangle_{\text{pol}} \otimes |L'_A\rangle_{e-t}, \quad (\text{S.2})$$

$$|V\rangle_{\text{pol}} \otimes |S_A\rangle_{e-t} \xrightarrow{\text{CNOT}} |V\rangle_{\text{pol}} \otimes |L'_A\rangle_{e-t}, \quad (\text{S.3})$$

$$|V\rangle_{\text{pol}} \otimes |L_A\rangle_{e-t} \xrightarrow{\text{CNOT}} |V\rangle_{\text{pol}} \otimes |S'_A\rangle_{e-t}. \quad (\text{S.4})$$

While the PBS swap the path mode depending on the polarisation state, they do not affect the time delays. In the delay histogram (see Fig. S6), this means that contributions are only shifted vertically (path domain), not horizontally

(time domain). Unlike the path labels before the bCNOT, the dashed path labels S'_A, L'_A, S'_B and L'_B after the bCNOT cannot be directly identified with a time delay, e.g. a photon detected in mode S'_A can, depending on the polarisation, either have been transmitted from path S_A or reflected from path L_A . For the path modes of the two photons, this means that while a photon pair in the modes S_A and S_B can be unambiguously assigned to the central-peak, a photon pair in the modes S'_A and S'_B can likewise originate from one of the side-peaks.

Let us now have a closer look on how the state illustrated in the histogram in Figure S6a evolves by the action of the bCNOT to the state illustrated by the histogram in Figure S6b. The polarisation state Φ^+_{pol} with a bit-flip admixture Ψ^+_{pol} can be described by the Bell-diagonal density matrix

$$\rho_{\text{pol}} = F_{\text{pol}}|\Phi^+\rangle_{\text{pol}}\langle\Phi^+| + (1 - F_{\text{pol}})|\Psi^+\rangle_{\text{pol}}\langle\Psi^+|, \quad (\text{S.5})$$

where F_{pol} is the polarisation fidelity. As demonstrated in Equation (S.1), an increased coincidence window introduces equal admixtures of a bit-flip error Ψ^+_{e-t} and a bit-phase-flip error Ψ^-_{e-t} to the e-t state, which can be described by the Bell-diagonal density matrix

$$\rho_{e-t} = F_{e-t}|\Phi^+\rangle_{e-t}\langle\Phi^+| + \frac{1 - F_{e-t}}{2} (|\Psi^+\rangle_{e-t}\langle\Psi^+| + |\Psi^-\rangle_{e-t}\langle\Psi^-|), \quad (\text{S.6})$$

with the e-t fidelity F_{e-t} . The tensor product of those two matrices $\rho = \rho_{\text{pol}} \otimes \rho_{e-t}$ describes the state of both DOF and has six non-zero entries in the Bell-diagonal form. For simplicity, the action of the bCNOT will be discussed on each of these six contributions separately.

Beforehand, let us clarify the action of the bCNOT with the help of an example. A photon pair in the $|H_A V_B\rangle$ state incident on both PBS from the short path is transformed as

$$|H_A V_B\rangle \otimes |S_A S_B\rangle \xrightarrow{\text{bCNOT}} |H_A V_B\rangle \otimes |S'_A L'_B\rangle. \quad (\text{S.7})$$

The polarisation remains unchanged and the path mode is flipped only if a photon is vertically polarised.

The state with both DOF in the Φ^+ state remains unchanged under the action of the bCNOT

$$|\Phi^+\rangle_{\text{pol}} \otimes |\Phi^+\rangle_{e-t} = \frac{1}{2} [|H_A H_B\rangle \otimes (|S_A S_B\rangle + |L_A L_B\rangle) + |V_A V_B\rangle \otimes (|S_A S_B\rangle + |L_A L_B\rangle)] \quad (\text{S.8a})$$

$$\xrightarrow{\text{bCNOT}} \frac{1}{2} [|H_A H_B\rangle \otimes (|S'_A S'_B\rangle + |L'_A L'_B\rangle) + |V_A V_B\rangle \otimes (|L'_A L'_B\rangle + |S'_A S'_B\rangle)] \quad (\text{S.8b})$$

$$= |\Phi^+\rangle_{\text{pol}} \otimes |\Phi^+\rangle_{e-t}. \quad (\text{S.8c})$$

This property makes the Φ^+ state the target state of the distillation scheme. The erroneous contributions in polarisation paired with the Φ^+_{e-t} state in the e-t DOF are transformed as

$$|\Psi^+\rangle_{\text{pol}} \otimes |\Phi^+\rangle_{e-t} = \frac{1}{2} [|H_A V_B\rangle \otimes (|S_A S_B\rangle + |L_A L_B\rangle) + |V_A H_B\rangle \otimes (|S_A S_B\rangle + |L_A L_B\rangle)] \quad (\text{S.9a})$$

$$\xrightarrow{\text{bCNOT}} \frac{1}{2} [|H_A V_B\rangle \otimes (|S'_A L'_B\rangle + |L'_A S'_B\rangle) + |V_A H_B\rangle \otimes (|L'_A S'_B\rangle + |S'_A L'_B\rangle)] \quad (\text{S.9b})$$

$$= |\Psi^+\rangle_{\text{pol}} \otimes |\Psi^+\rangle_{e-t}. \quad (\text{S.9c})$$

After the bCNOT, these contributions are discarded by the postselection on the Φ^{\pm}_{e-t} states in energy-time. The postselection projector reads

$$P_{\Phi^{\pm}} = \mathbb{1}_{\text{pol}} \otimes (|\Phi^+\rangle_{e-t}\langle\Phi^+| + |\Phi^-\rangle_{e-t}\langle\Phi^-|) = \mathbb{1}_{\text{pol}} \otimes (|S'_A S'_B\rangle\langle S'_A S'_B| + |L'_A L'_B\rangle\langle L'_A L'_B|). \quad (\text{S.10})$$

Similarly, the side-peaks are transformed as

$$|\Phi^+\rangle_{\text{pol}} \otimes |S_A L_B\rangle \xrightarrow{\text{bCNOT}} |H_A H_B\rangle \otimes |S'_A L'_B\rangle + |V_A V_B\rangle \otimes |L'_A S'_B\rangle, \quad (\text{S.11})$$

$$|\Phi^+\rangle_{\text{pol}} \otimes |L_A S_B\rangle \xrightarrow{\text{bCNOT}} |H_A H_B\rangle \otimes |L'_A S'_B\rangle + |V_A V_B\rangle \otimes |S'_A L'_B\rangle. \quad (\text{S.12})$$

As the coincidence window is widened, the non-interfering background can be described as a mixture of Bell states as noted in Equation (S.6). While the transformation of those contributions is completely described by Equations (S.11) and (S.12), it can be rephrased in the Bell basis as

$$|\Phi^+\rangle_{\text{pol}} \otimes |\Psi^+\rangle_{e-t} \xrightarrow{\text{bCNOT}} |\Phi^+\rangle_{\text{pol}} \otimes |\Psi^-\rangle_{e-t}, \quad (\text{S.13})$$

$$|\Phi^+\rangle_{\text{pol}} \otimes |\Psi^-\rangle_{e-t} \xrightarrow{\text{bCNOT}} |\Phi^-\rangle_{\text{pol}} \otimes |\Psi^-\rangle_{e-t}. \quad (\text{S.14})$$

In this case, contributions from the target state in polarisation are discarded in postselection. In contrast, erroneous polarisation contributions that are within the increased coincidence window, are kept in postselection. The side-peaks transform like

$$|\Psi^+\rangle_{\text{pol}} \otimes |S_A L_B\rangle \xrightarrow{\text{bcNOT}} |H_A V_B\rangle \otimes |S'_A S'_B\rangle + |V_A H_B\rangle \otimes |L'_A L'_B\rangle, \quad (\text{S.15})$$

$$|\Psi^+\rangle_{\text{pol}} \otimes |L_A S_B\rangle \xrightarrow{\text{bcNOT}} |H_A V_B\rangle \otimes |L'_A L'_B\rangle + |V_A H_B\rangle \otimes |S'_A S'_B\rangle, \quad (\text{S.16})$$

which can be expressed for the contributions included in the coincidence window as

$$|\Psi^+\rangle_{\text{pol}} \otimes |\Psi^+\rangle_{\text{e-t}} \xrightarrow{\text{bcNOT}} |\Psi^+\rangle_{\text{pol}} \otimes |\Phi^+\rangle_{\text{e-t}}, \quad (\text{S.17})$$

$$|\Psi^+\rangle_{\text{pol}} \otimes |\Psi^-\rangle_{\text{e-t}} \xrightarrow{\text{bcNOT}} |\Psi^-\rangle_{\text{pol}} \otimes |\Phi^-\rangle_{\text{e-t}}. \quad (\text{S.18})$$

We showed that widening the coincidence window does indeed have the desired effect of creating a mixed state in the energy-time degree of freedom. Further, we discussed a distillation step including joint action of the polarising beams splitters as well as the postselection in detail and illustrated how the proportion of unwanted contribution to the target state in polarisation is thereby reduced.

Appendix E: Comparison of distillation rates

In the main text, we compare the single-copy distillation rate with the two-copy distillation rate [23]. In Table I we list the most relevant contributions to the distillation rate for the two protocols, starting from the photon-pair creation with pulsed SPDC sources and the subsequent transmission over a dual link, to the distillation operation itself. Further rate-diminishing factors in the two-copy distillation protocol, such as inefficient quantum memories [49] and inherently probabilistic CNOT gates [21], are not included in this table.

TABLE I. Comparison of distillation rates between single-copy and two-copy entanglement distillation. The pulsed SPDC source used in the two-copy distillation experiment [23] produces a mean number of photon pairs per pulse of $p = 0.00022$ at a repetition rate of $R_{\text{rep}} = 76$ MHz. We assume a link transmittance of $t = -20$ dB and a yield of $Y = 0.8$.

Distillation scheme	Creation probability	Transmission probability	Protocol yield	Distillation rate [1/s]
Single copy	p	t^2	Y	$R_{\text{rep}} p t^2 Y = 1.36$
Two copy	p^2	t^4	$Y/2$	$R_{\text{rep}} p^2 t^4 Y/2 = 1.52 \cdot 10^{-8}$